Benzimidazole linked polymers (BILPs) in mixed-matrix membranes

Influence of filler porosity on the CO_2/N_2 separation performance

Shan, Meixia; Seoane, Beatriz; Pustovarenko, Alexey; Wang, Xuerui; Liu, Xinlei; Yarulina, Irina; Abou-Hamad, Edy; Kapteijn, Freek; Gascon, Jorge

DOI
10.1016/j.memsci.2018.08.023

Publication date
2018

Document Version
Accepted author manuscript

Published in
Journal of Membrane Science

Citation (APA)
Shan, M., Seoane, B., Pustovarenko, A., Wang, X., Liu, X., Yarulina, I., Abou-Hamad, E., Kapteijn, F., & Gascon, J. (2018). Benzimidazole linked polymers (BILPs) in mixed-matrix membranes: Influence of filler porosity on the CO_2/N_2 separation performance. *Journal of Membrane Science*, *566*, 213-222. https://doi.org/10.1016/j.memsci.2018.08.023

Benzimidazole linked polymers (BILPs) in mixed-matrix membranes: ~~influence~~Influence of filler porosity on the CO_2/N_2 separation performance

Meixia Shan[a]

Beatriz Seoane[b]

b.seoanedelacuesta@uu.nl

Alexey Pustovarenko[c]

Xuerui Wang[a]

Xinlei Liu[a]

Irina Yarulina[c]

Edy Abou-Hamad[d]

Freek Kapteijn[a]

Jorge Gascon[a, c]

jorge.gascon@kaust.edu.sa

[a]Catalysis Engineering, Chemical Engineering Department, Delft University of Technology, van der Maasweg, ~~9~~9, 2629 HZ Delft, The Netherlands

[b]Inorganic Chemistry and Catalysis group, Debye Institute for Nanomaterials Science, Utrecht University, Universiteitsweg ~~99~~99, Utrecht 3584 ~~CG~~CG, The Netherlands

[c]King Abdullah University of Science and Technology, KAUST Catalysis Center, Advanced Catalytic ~~Materials.~~Materials, Thuwal ~~23955~~23955, Saudi Arabia

[d]King Abdullah University of Science and Technology (KAUST), Core Labs, Thuwal 23955-6900, Saudi Arabia

Abstract

The performance of mixed-matrix membranes (MMMs) based on ~~Matrimid®~~Matrimid® and benzimidazole-linked polymers (BILPs) have been investigated for the separation CO_2/N_2 and the dependency on the filler porosity. BILPs with two different porosities (BILP-101 and RT-BILP-101) were synthesized through controlling the initial polymerization rate and further characterized by several techniques (DRIFTs, ^{13}C CP/MAS NMR, SEM, TEM, N_2 and CO_2 adsorption). To investigate the influence of porosity, the two types of fillers were incorporated into ~~Matrimid®~~Matrimid® to prepare MMMs at varied loadings (8, 16 and ~~24~~24 wt%). SEM confirmed th~~e~~at both ~~well dispersion of~~ BILP-101 and RT-BILP-101 are well dispered, indicating their good compatibility with the polymeric matrix. The partial pore blockage in the membrane was verified by CO_2 adsorption isotherms on the prepared membranes. In the separation of CO_2 from a 15:85 CO_2:N_2 mixture at ~~308~~308 K, the incorporation of both BILPs fillers resulted in an enhancement in gas permeability together with constant selectivity owing to the fast transport pathways introduced by the porous network. It was noteworthy that the initial porosity of the filler had a large impact in separation permeability. The best improvement was achieved by ~~24~~24 wt% RT-BILP-101 MMMs, for which the CO_2 permeability increases up to 2.8-fold (from 9.6 to 27 Barrer) compared to the bare ~~Matrimid®.~~Matrimid®.

Keywords: Benzimidazole-linked polymers; Mixed-matrix membranes; CO_2 separation

1 Introduction

The soaring increase in CO_2 emissions has caused great public concern due to its accompanying greenhouse effect. In this sense, the capture of CO_2 from flue gas or natural gas has become necessary from the perspective of energy and the environment [1]. ~~Flue gas is composed of CO~~Flue gas is composed of CO~~$_2$~~$_2$~~, N~~, N~~$_2$~~$_2$~~, CO, O~~, CO, O~~$_2$~~$_2$~~, water vapor and sulfur oxide, where N~~, water vapor and sulfur oxide, where N~~$_2$~~$_2$ ~~and CO~~and CO~~$_2$~~$_2$ ~~are the main components with a~~

~~CO~~are the main components with a CO~~$_2$~~$_2$~~/N~~/N~~$_2$~~$_2$ ~~ratio around 15:85.~~ ratio around 15:85. Traditional technologies using amines or solvents to absorb CO_2 are environmentally unfriendly and energy intensive. Membrane-based gas separation on the other hand is a promising alternative owing to its attractive features, such as smaller footprints, easy operation and energy efficiency. Although many novel membrane materials have been proposed, polymeric membranes still dominate the current membrane market given their good processability, mechanical stability and low price. Nevertheless, conventional polymeric membranes suffer from a universal 'trade-off' relation between permeability and selectivity, known as the Robeson upper bound [2,3]. Extensive efforts have been devoted to improve the gas separation performance (permeability and selectivity) of polymeric membranes, which include polymer blending [4], post-treatment of the membranes via cross-linking [5] or thermal rearrangement [6] and the development of novel nanoporous polymers, such as polymers of intrinsic microporosity (PIMs) [7,8]. In this line, one of the most promising approaches to overcome polymers' gas separation performance is to use mixed-matrix membranes (MMMs), consisting of a blend of selected fillers dispersed in a continuous polymeric matrix. This strategy allows to combine into one membrane the better separation performance of the selected fillers with the good processability and low price of polymeric membranes. Numerous porous fillers such as zeolites [9,10] and ~~M~~metal-~~O~~organic ~~F~~frameworks (MOFs) [11,12] have been successfully incorporated into different polymers to prepare MMMs, resulting in an improved separation performance compared to the bare polymer membranes.

Porous organic frameworks (POFs) [13], such as covalent organic frameworks (COFs) [14,15], conjugated microporous polymers (CMPs) [16], porous aromatic frameworks (PAFs) [17] and covalent triazine-based frameworks (CTFs) [18], are a relatively new category of porous materials constructed from covalent bonds. Given their diversified porosities, tunable chemical properties, inherent light weight and exceptional chemical and thermal stabilities, POFs are promising candidates to be used as fillers in MMMs for CO_2 separation [19,20]. For example, Jin ~~et al~~et al. [21] studied the effect of dispersing COF nanosheets in polyether-block-amide (PEBA) and prepared PEBA-based MMMs, which showed a 56% improvement in the ideal selectivity towards CO_2/N_2 compared to the pure PEBA membrane with only 1 wt% COF loading. Zhu ~~et al~~et al. [22] developed a new synthesis protocol to prepare self-supported PAF-56P@PSF composite hollow fibre membranes with a CO_2 over N_2 selectivity of 38.9 together with good thermal and mechanical stabilities. Recently, our group incorporated ACOF-1 in three different polymers to prepare MMMs for CO_2 separation [23]. The best improvement was observed for Matrimid®-based MMMs, for which a 20% and 87% increase in CO_2/N_2 selectivity and CO_2 permeability, respectively, was obtained for 16 wt% COF loading~~, respectively~~. These examples underscore the compatibility between POFs with different polymer matrices resulting in MMMs with improved performance when compared to the pure polymers. The fully organic nature of POFs has been reported to account for this good compatibility, in contrast to other inorganic fillers, such as zeolites, for which a poor compatibility resulting in the formation of voids at the filler-polymer interface has often been encountered.

Benzimidazole-linked polymers (BILPs) were first reported in 2011 [24]. BILPs have shown high CO_2 uptakes (up to ~ 6 mmol g^{-1} at 273 K for BILP-19 [25]) together with high CO_2/N_2 and CO_2/CH_4 adsorption selectivities [26]. This preference for CO_2 has been related to the presence of imidazole functionalities in the POF framework. Further, the excellent thermal and chemical stabilities of BILPs make them desirable for practical separations. Sekizkardes ~~et al~~et al. [27] successfully incorporated BILP-101 nanoparticles into the high free volume PIM-1 matrix. The obtained MMMs achieved a 53% enhancement in the CO_2 permeability together with good stability under harsh conditions upon 30 wt% POF loading, ~~further p~~proving the feasibility of using BILPs as fillers in~~ the~~ the preparation of MMMs.

In terms of fillers, porosity is an important factor affecting their CO_2 uptake and selectivity~~, playing a key role on the MMMs performance~~ [28,29]. Several studies have been devoted to the influence of the filler particle size and morphology [12,30–33] as well as filler functionalities [34] on the membrane performance. However, the role of the fillers' porosity has remained largely unexplored. Herein, therefore, the effect of filler porosity on the separation performance of POFs-containing MMMs is studied. BILP-101 particles with different porosities were synthesized by controlling the initial polymerization rate and used as fillers in the polyimide ~~Matrimid®~~Matrimid® 5218. ~~Matrimid®~~Matrimid® 5218 was chosen as polymer matrix owing to its good CO_2 selectivity together with its high thermal and chemical stabilities and commercial availability. The prepared membranes were tested for CO_2/N_2 separation at ~~308~~308 K and the effect of filler porosity, filler loading, and feed pressure on membrane performance was assessed.

2 Experimental ~~Section~~section

2.1 Materials

Benzene-1,3,5-tricarboxaldehyde (97%), 1,2,4,5-benzenetetramine tetrahydrochloride, hydrochloric acid (37%), sodium hydroxide (99.99% metals basis), acetone (99.9%) and tetrahydrofuran (THF, 99.9%) were purchased from Sigma Aldrich. N,N-Dimethylformamide (DMF, 99.8%, extra dry over molecular sieves) was purchased from Thermo Fisher. All these starting materials and solvents were used without further purification. Matrimid® 5218 ($M_w \approx$ 123,000 g mol~~$^{-1}$~~$^{-1}$, $M_n \approx$ 11,000 g mol~~$^{-1}$~~$^{-1}$) was kindly supplied by Huntsman Advanced Materials. Matrimid® was dried prior to use to remove the adsorbed moisture under vacuum at 453 K for 48 h.

2.2 Synthesis of BILP-101 and RT-BILP-101

BILP-101 was synthesized following the same procedure as previously reported by Sekizkardes ~~et al~~et al. [35] In a typical synthesis, a 100 mL round bottom flask was charged with 1,2,4,5-benzenetetramine tetrahydrochloride (100 mg, 0.35 mmol), 60 mL anhydrous DMF, and a stirring bar. The resultant homogeneous solution was degassed under N_2 for 1 h, cooled to approximately 243 K and treated drop-wise with a solution of 1,3,5-triformylbenzene (40 mg, 0.23 mmol) in anhydrous DMF (15 mL). The temperature was maintained at *ca.* 243 K for 1 h during which a dark-brown solid formed. The resultant slurry solution was then left to warm to room temperature overnight, flushed with air for 30 min, and further heated to 403 K in an oven, temperature at which the reaction mixture was kept for 2 days. The solid was then collected by centrifugation at 5,000 rpm for 10 min for 2 cycles and subsequently washed with DMF, acetone, water, 1 M HCl, 1 M NaOH, water and acetone. Finally, the product was dried overnight at 393 K under vacuum.

RT-BILP-101 was prepared following the same procedure as described for BILP-101, but without the low temperature treatment, *i.e.,* 1,3,5-triformylbenzene was added to the 1,2,4,5-benzenetetramine tetrahydrochloride solution at room temperature (Scheme 1).

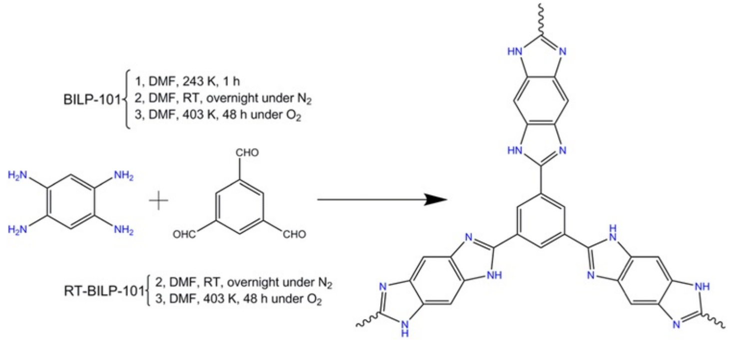

Scheme 1 Schematic of the procedure followed for the synthesis of BILP-101 and RT-BILP-101.

alt-text: Scheme 1

2.3 Preparation of mixed-matrix membranes (MMMs)

To prepare the MMMs, the required amount of BILP-101 particles (or RT-BILP-101) was first dispersed in THF and sonicated for ~~30~~30 min. To this suspension, ~~0.2~~0.2 g of dried ~~Matrimid®~~Matrimid® was added and the casting suspension was further stirred overnight. The solvent/filler-polymer weight ratio was kept at 90/10 in all cases. The amount of BILP-101 in the casting suspension was adjusted to achieve the desired final filler loading of ~~8~~8 wt%,~~wt.%,~~ ~~16~~ 16 wt% and ~~24~~24 wt% in the resulting MMMs.

The prepared suspensions were then casted onto a clean glass plate with the help of a Doctor Blade knife. The cast membranes were immediately covered with a small watch glass to prevent too fast evaporation of the solvent. The glass plate was further covered with a square box ~~and~~together with four small vials containing THF to create a saturated THF atmosphere. All these measures were taken to slow down the evaporation rate of THF, thereby preventing the formation of defects during membrane drying. The membranes were first left to dry overnight at room temperature and then dried under vacuum for ~~24~~24 h at ~~423~~423 K.

The pure polymer membranes were prepared following the same procedure as the MMMs, but without the extra step of dispersing BILP-101 or RT-BILP-101 particles. The final thickness of the resulting membranes was the average value of several measurements from various positions individually evaluated by a digital micrometer (Mitutoyo, IP54 Absolute Digimatic Micrometer, MDQ-30, range ~~0–30~~0–30 mm,~~mm, accuracy ±0.001~~ accuracy ± 0.001 mm).

2.4 Filler and membrane characterization

Diffuse Reflectance Infrared Fourier transform (DRIFT) spectra of BILP-101 and RT-BILP-101 powders were acquired in a Nicolet 8700 FT-IR (Thermo Scientific) spectrometer equipped with a high temperature cell with CaF_2 windows. The samples were pretreated in a He flow at ~~393~~393 K for ~~5~~5 min prior to collecting the spectra.

One-dimensional ^{13}C CP/MAS solid state NMR spectra were recorded on a Bruker AVANCE III spectrometer operating at ~~600~~600 MHz resonance frequencies for ^{1}H. Experiments at ~~600~~600 MHz employed a conventional double-resonance ~~3.2~~3.2 mm CP/MAS probe or a ~~2.5~~2.5 mm double-resonance probe. Dry nitrogen gas was used for sample spinning to prevent degradation. NMR chemical shifts are reported with respect to the external references ~~TMS~~tetramethylsilane and adamantane. For ^{13}C CP/MAS NMR experiments, the following sequence was used: 90° pulse on the proton (pulse length ~~2.4~~2.4 s), then a cross-polarization step with contact time of typically ~~2 ms,~~ 2 ms, and finally acquisition of the ^{13}C NMR signal under high-power proton decoupling. The delay between the scans was set to ~~5~~5 s to allow the complete relaxation of the ^{1}H nuclei, and the number of scans ranged between 10,000 and 20,000. An exponential apodization function corresponding to a line broadening of ~~80~~80 Hz was applied prior to Fourier transformation. The sample spinning frequency was ~~15~~15 kHz and ~~20 KHz.~~20 kHz.

Powder X-Ray Diffraction (PXRD) patterns of BILP-101 and RT-BILP-101 were recorded using a Bruker-D8 Advanced diffractometer with Co-K_α radiation ($\lambda = 1.78897$ Å). The samples were scanned in the 2~~-~~θ range of 5–80° using a step size of 0.02° and a scan speed of 0.4 s per step in a continuous scanning mode.

Scanning Electron Microscopy (SEM) micrographs were acquired using a JEOL JSM-6010LA InTouchScope microscope equipped with an integrated SDD EDS detector. BILP-101 and RT-BILP-101 particles were directly put on the sample holder and cross-section of the prepared membranes were obtained by cryo-fracturing in liquid nitrogen. All the samples were sputtered with gold for ~~60~~60 s prior to acquiring SEM micrographs.

N_2 physisorption ~~(77~~(77 K) and CO_2 adsorption isotherms ~~(273~~(273 K) of BILP-101, RT-BILP-101 and the resulting MMMs were recorded in a Tristar II 3020 (Micromeritics). ~~Argon adsorption isotherm was performed in 3Flex (Micromeritics) instrumentA.~~ Argon adsorption isotherm was performed in 3Flex (Micromeritics) instrument. Prior to the gas adsorption measurements, the samples were degassed at ~~423~~423 K under N_2 flow for ~~16~~16 h to remove any solvent or moisture trapped in the polymer network. ~~The pore size distribution (PSD) curves of the prepared BILPs fillers and corresponding MMMs was estimated by CO~~The pore size distribution (PSD) curves of the prepared BILPs fillers and corresponding MMMs was estimated by $CO_{\cancel{2}2}$ ~~DFT (Density functional theory) model, using a non-negative regularization method with a factor of 0.03160. The standard deviation of the fit is 0.002057, 0.001954, 0.001904 and 0.002594mmol g~~-DFT (Density functional theory) model, using a non-negative regularization method with a factor of 0.03160. The standard deviation of the fit is 0.002057, 0.001954, 0.001904 and 0.002594 mmol $g^{\cancel{-1}-1}$ ~~for RT-BILP-101, BILP-101, 16wt.% BILP-101 MMMs and 16wt.% RT-BILP-101 MMMs, respectively. For the PSD calculation based on Ar adsorption, a Non Local DFT (NLDFT) model was employed with the assumption of cylindrical pores, using a non-negative regularization method with a factor of 0.03160. The standard deviation of the fit is 0.36770 and 0.52406cm~~for RT-BILP-101, BILP-101, 16 wt% BILP-101 MMMs and 16 wt% RT-BILP-101 MMMs, respectively. For the PSD calculation based on Ar adsorption, a Non Local DFT (NLDFT) model was employed with the assumption of cylindrical pores, using a non-negative regularization method with a factor of 0.03160. The standard deviation of the fit is 0.36770 and 0.52406 $cm^{\cancel{3}3}$~~(STP) g~~(STP) $g^{\cancel{-1}-1}$ ~~for BILP-101 and RT-BILP-101, respectively.~~for BILP-101 and RT-BILP-101, respectively.

Thermogravimetric analyses (TGA) were performed in a Mettler Toledo TGA/SDTA851e apparatus by measuring the mass loss of the sample while heating BILPs and the prepared membranes under air flow ~~(100~~(100 mL $min^{\cancel{-1}-1}$) from room temperature to ~~1073~~1073 K at a heating rate of ~~5~~5 K $min^{\cancel{-1}-1}$.

Differential Scanning Calorimetry (DSC) measurements were carried out using a Perkin Elmer DSC 7 equipment to assess the glass transition temperature (T_g) of the neat membrane and the MMMs. The scanning range was 298–698 K at a heating rate of 10 K $min^{\cancel{-1}-1}$ under nitrogen atmosphere. Two consecutive runs were performed. ~~A~~The first DSC cycle was performed to remove thermal history and adsorbed water from the samples. After cooling, a second cycle was performed following the same procedure. The glass transition temperature (T_g) value was calculated as the middle point of the slope transition in the DSC curve.

2.5 Gas permeation experiments

Membrane areas of 3.14 cm^2 were cut from the casted membrane films, placed on a macroporous support and mounted in a flange between Viton® o-rings. This flange fits in a permeation module, which was placed inside an oven in the permeation home-made setup described elsewhere [36]. The CO_2/N_2 separation measurements were performed employing a 15:85 CO_2:N_2 gas mixture (23 mL $min^{\cancel{-1}-1}$ CO_2 and 130 mL $min^{\cancel{-1}-1}$ of N_2) as feed. Helium (4.6 mL $min^{\cancel{-1}-1}$) was used as sweep gas at the permeate side. The absolute pressure of the feed stream was adjusted in a range of 2–5 bar using a back-pressure controller at the retentate side, while keeping the permeate side at atmospheric pressure. ~~The temperature in the permeation module was kept at 308K when collecting the data at different feed pressures for fresh membranes. The aged membranes were first tested at different feed pressures (up to 5bar) and then at different temperatures,~~The temperature in the permeation module was kept at 308 K when collecting the data at different feed pressures for fresh membranes. The aged membranes were first tested at different feed pressures (up to 5 bar) and then at different temperatures, ~~*i.e.*~~*i.e.* ~~308, 323 and 353K, at 2bar.~~308, 323 and 353 K, at 2 bar.

An on-line gas chromatograph (Interscience Compact GC) equipped with a packed Carboxen 1010 PLOT ~~(30~~(30 m × 0.32 mm) column and TCD detector was used to periodically analyse the permeate stream. Each membrane was fabricated and measured 2–3 times to ensure reproducibility of the reported data. In all cases, gas separation performance was evaluated after ensuring steady operation.

Gas separation performance was defined by the separation factor (α) and the gas permeability (P) of the individual components. The permeability for the i-component (P_i) was calculated as follows (Eq. (1)):

$$P_i = \frac{F_i \cdot l}{\Delta p_i \cdot A} \qquad \textbf{(1)}$$

where F_i denotes the molar flow rate of compound i, l is the thickness of the membrane measured by a digital micrometer and A is the membrane area. Δp_i is the partial pressure difference of the component i across the membrane and it can be calculated according to Eq. (2).

$$\Delta p_i = p_{feed} \times Y_{i,\ \ feed} - p_{perm} \times X_{i,\ \ perm} \qquad \textbf{(2)}$$

where p_{feed} *and* p_{perm} represent the pressures at the feed and permeate sides and $Y_{i,\ feed}$ and $X_{i,\ perm}$ are the molar fractions of the component i in the feed and permeate gas streams, respectively.

The SI unit for the permeability is ~~mol s~~mol $s^{\cancel{-1}-1}$ ~~m~~ $m^{\cancel{-1}-1}$ ~~Pa~~ $Pa^{\cancel{-1}-1}$. However, gas permeabilities are commonly reported in the widely used non-SI unit Barrer, where 1 ~~Barrer=3.35×10~~Barrer = 3.35 × 10^{-16}~~mol s~~ mol $s^{\cancel{-1}-1}$~~m~~ m$^{\cancel{-1}-1}$~~Pa~~ $Pa^{\cancel{-1}-1}$.

The separation factor or mixed gas selectivity (α) was calculated as the ratio of the permeability of the more permeable compound (CO_2) to the permeability of the less permeable compound (N_2) (Eq. (3)).

$$\alpha = \frac{P_{CO2}}{P_{N2}} \qquad \textbf{(3)}$$

3 Results and discussion

3.1 Characterization of BILP-101 and RT-BILP-101

BILP-101 particles were synthesized by a condensation reaction following the synthetic route recently ~~developed~~ reported for BILP [26,35,37]. This approach requires the slow addition of aldehyde at low temperatures (243 K) during the initial polymerization stages to control the overall porosity of the final product (*vida supra*). In this work, we synthesized two different POFs: BILP-101 and RT-BILP-101. BILP-101 was obtained following the procedure previously reported by Sekizkardes ~~et al~~et al. [35], in which the 1,2,4,5-benzenetetramine tetrahydrochloride solution was cooled to 243 K prior to drop-wise adding the aldehyde-containing solution (see experimental section). Aiming at tuning the polymer porosity, RT-BILP-101 was prepared following the same procedure as described for BILP-101, but at room temperature (Scheme 1). This influences the early stages of the condensation reaction, a~~ffecting~~ltering the initial polymerization rate and ultimately affect~~s~~ing the porosity of the resulting product.

Both products were characterized by DRIFTS, solid-state ^{13}C cross-polarization magic-angle spinning (CP/MAS) NMR spectroscopy, XRD and N_2 and CO_2 adsorption. The DRIFT spectra acquired for BILP-101 and RT-BILP-101 (Fig. 1a) indicate the same chemical connectivity for these two polymers and confirmed the imidazole ring formation. Particularly, the bands at 1611 cm~~$^{-1}$~~$^{-1}$ (-C=N-) and 1499 and 1440 cm^{-1} (assigned to the skeleton vibration of the imidazole ring) [26,38] point to the successful imidazole ring closure upon poly-condensation. These observations are further supported by the bands at 1362 cm^{-1} (C-N stretching) and 1641 cm^{-1} (N-H bending), which confirmed the formation of the benzimidazole ring. Also, the absence of a band at 1700 cm~~$^{-1}$~~$^{-1}$, which could be ascribed to the residual C=O stretching of the aldehyde moieties, points to a complete consumption of the starting aldehyde functional groups. This was corroborated by ^{13}C CP-MAS NMR spectroscopy. For both materials, BILP-101 and RT-BILP-101, the ^{13}C CP-MAS NMR spectra show a peak at $\delta = 151$ ppm (Fig. 1b), corresponding to the N=C-N imidazole carbon.

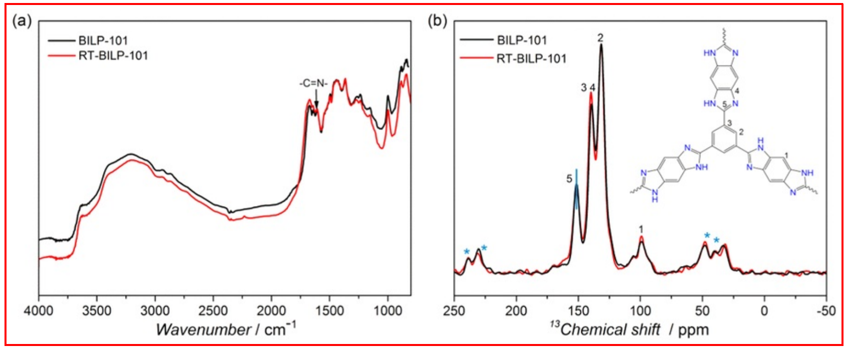

Fig. 1 ~~(a)~~(a) DRIFT spectra of BILP-101 and RT-BILP-101 acquired at ~~393~~393 K under He atmosphere and (b) assignments of the ^{13}C CP-MAS NMR spectra obtained for BILP-101 and RT-BILP-101.

alt-text: Fig. 1

The thermal stability of BILP-101 and RT-BILP-101 was supported by TGA under air atmosphere. The results show that BILP-101 and RT-BILP-101 are stable up to ~~635~~635 K (Fig. S1), while the initial weight losses, before ~~373~~373 K, can be attributed to the removal of the adsorbed moisture. Transmission electron and scanning electron microscopy micrographs (Figs. 2a and b, 3a and 4a) reveal the formation of homogenous spherical-shaped particles for both BILP-101 and RT-BILP-101. In the case of RT-BILP-101, however, a decrease in the particle size can be observed compared to BILP-101 (from ~~240 ± 10~~240 ± 10 nm to ~~310 ± 10~~310 ± 10 nm, for the former and the latter case, respectively, Fig. 2c and d). We relate this to the higher initial reaction rate at room temperature than at ~~243~~243 K, favouring nucleation and resulting in the observed decrease of particle size. As expected, both BILPs are amorphous as determined by powder X-ray diffraction (Fig. S2).

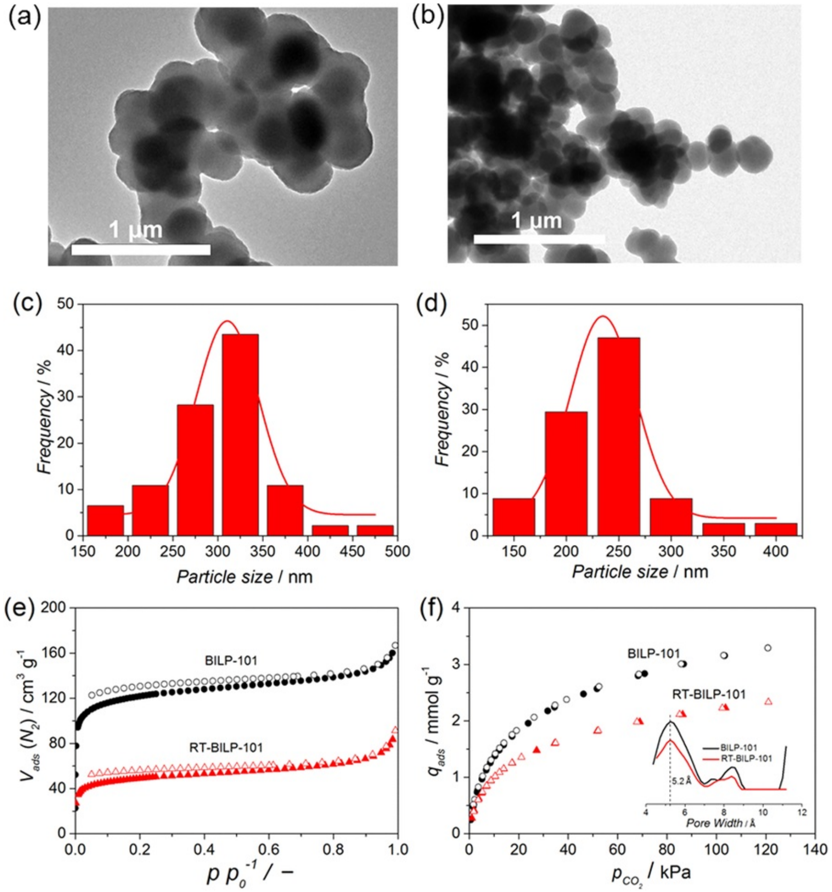

Fig. 2 TEM micrographs (a and b)~~,~~ and particle size distribution (c and d) of BILP-101 and RT-BILP-101, respectively. N_2 (e) and CO_2 (f) adsorption / desorption isotherms of BILP particles. Closed symbols represent the adsorption and open symbols represent the desorption branches. ~~Black and red correspond to BILP-101 and RT-BILP-101, respectively. Inset in (f) shows the pore size distribution (PSD) of BILP-101 and RT-BILP-101 calculated from the CO~~Black and red correspond to BILP-101 and RT-BILP-101, respectively. Inset in (f) shows the pore siz

distribution (PSD) of BILP-101 and RT-BILP-101 calculated from the CO~~2~~2 ~~adsorption isotherms.~~adsorption isotherms.

alt-text: Fig. 2

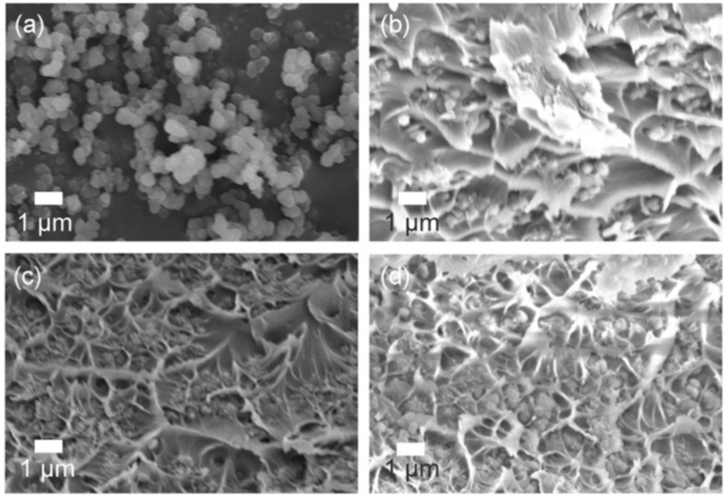

Fig. 3 SEM micrographs of (a) BILP-101 and the cross-section of (b) ~~8~~8 wt%~~wt.% BILP-101@Matrimid®,~~ BILP-101@Matrimid®, (c) ~~16~~16 wt%~~wt.% BILP-101@Matrimid®~~ BILP-101@Matrimid® and (d) ~~24~~24 wt%~~wt.% BILP-101@Matrimid®.~~ BILP-101@Matrimid®.

alt-text: Fig. 3

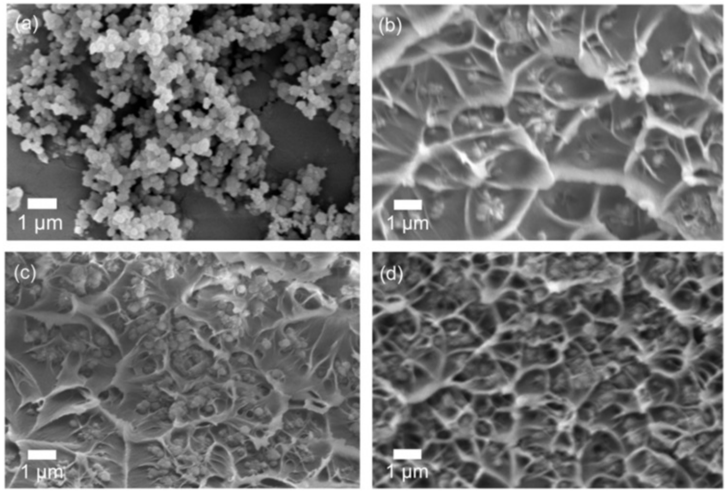

Fig. 4 SEM micrographs of (a) RT-BILP-101 and the cross-section of (b) ~~8~~8 wt%~~wt.% RT-BILP-101@Matrimid®,~~ RT-BILP-101@Matrimid®~~,~~ (c) ~~16~~16 wt%~~wt.% RT-BILP-101@Matrimid®~~ RT-BILP-101@Matrimid® and (d) ~~24~~24 wt%~~wt.% RT-BILP-101@Matrimid®.~~ RT-BILP-101@Matrimid®.

alt-text: Fig. 4

BILPs' porosity was investigated via N_2 adsorption acquired at 77 K (Fig. 2e). The isotherms exhibit a steep uptake at low relative pressures ($p/p_o < 0.1$), indicating the microporous nature of the two prepared polymers. The calculated Brunauer-Emmett-Teller (BET) areas of BILP-101 and RT-BILP-101 are 460 and 180 m^2 g~~$^{-1}$~~$^{-1}$, respectively. As expected, BILP-101 possesses a higher BET surface area, which can indeed be ascribed to its slower initial formation rate (*vide supra*)~~,~~. This slower initial polymerization prevent~~ing~~s the premature precipitation of oligomers during the initial polymerization stages and allow~~ing~~s for a better pore formation resulting in an overall enhanced porosity [39,40]. Furthermore, Fig. 2f shows the low-pressure CO_2 adsorption isotherms acquired for RT-BILP-101 and RT-BILP-101~~ acquired~~ at 273 K. At 1 bar, the CO_2 uptake observed for BILP-101 reach up to 3.2 mmol g~~$^{-1}$~~$^{-1}$, which is comparable to other POFs [26,41–45]. RT-BILP-101 on the other hand exhibits relatively lower CO_2 adsorption capacity (2.2 mmol g~~$^{-1}$~~$^{-1}$ at 1 bar and 273 K), in line with N_2 adsorption results. The inset in Fig. 2f presents the pore size distribution (PSD) curves calculated from the adsorption branch of the CO_2 isotherms. ~~Both BILPs show a bimodal pore structure with pores centered around 5.2Å and a broader range of pores between~~Both BILPs show a bimodal pore structure with pores centered around 5.2 Å and a broader range of pores between ~~*ca*~~*ca*~~*. 7 and 9Å. BILP-101 presents more open pore volume than RT-BILP-101, being more prone to the penetration of the polymer chains, as discussed below.*~~. 7 and 9 Å. BILP-101 however ~~presents~~possesses more open pore volume than RT-BILP-101, being more prone to the penetration of the polymer chains, as discussed below.

All in all, two different BILPs were successfully synthesized with the same chemical connectivity, but with different textural properties. This was achieved by tuning the temperature in the early polymerization stages, influencing the initial reaction rate and allowing for a certain degree of control over the overall BILP porosity. ~~In order to further evaluate the potential of these two BILPs for post-combustion CO~~In order to further evaluate the potential of these two BILPs for post-combustion CO~~2~~$_2$ ~~capture, the adsorption selectivities of CO~~capture, the adsorption selectivities of CO~~2~~$_2$~~/N~~/N~~2~~$_2$ ~~were calculated using the initial slope method.~~were calculated using the initial slope method. Fig. S4 ~~shows that BILP-101 and RT-BILP-101 have a CO~~shows that BILP-101 and RT-BILP-101 have a CO~~2~~$_2$~~/N~~/N~~2~~$_2$ ~~selectivity of 89 and 60 at 273K, respectively. These results are in line with reported values~~selectivity of 89 and 60 at 273 K, respectively. These results are in line with reported values [35] ~~and demonstrate that BILP-101 and RT-BILP-101 are promising fillers for the preparation of MMMs for CO~~and demonstrate that BILP-101 and RT-BILP-101 are promising fillers for the preparation of MMMs for CO~~2~~$_2$~~/N~~/N~~2~~$_2$ ~~separation.~~separation.

3.2 Characterization of BILPs MMMs

In order to study the influence of the filler porosity on the performance of MMMs in gas separation, MMMs were prepared with both BILP-101 and RT-BILP-101 particles. SEM micrographs of the ~~surface (~~surface (Fig. S5~~)~~) and cross-section (Figs. 3 and 4) of the prepared membranes were acquired. The images show that both BILP-101 and RT-BILP-101 are randomly dispersed in the polymer matrix at low weight loading ~~(8~~(8 wt%) and began to undergo slight~~ly~~ aggregation at higher loadings. No evident interfacial voids or pinholes could be observed even at ~~24~~24 wt% BILP loading. In addition, both fillers retain their spherical morphology upon membrane preparation. In comparison with BILP-101 MMMs, RT-BILP-101 MMMs exhibit better filler dispersion and a more integrated morphology, where RT-BILP-101 particles are uniformely wrapped by the polymer chains~~ are observed~~. Fig. S6 presents the thermogravimetric analys~~e~~is (TGA) ~~acquired~~ for the bare ~~Matrimid®~~Matrimid® ~~membranes~~ together with those obtained for the BILP-101 and RT-BILP-101-based MMMs. The TGA results of BILP-101 and RT-BILP-101 were also included for comparison. As mentioned above, BILP-101 and RT-BILP-101 were stable up to ~~635~~635 K, temperature at which ~~i~~they~~t~~ start~~s~~ decomposing. This decomposition temperature is higher for the pure ~~Matrimid®~~Matrimid® and the resulting MMMs for which decomposition starts at around ~~750~~750 K. ~~Further, the absence of weight loss at lower temperatures, for both MMMs and pure membranes, ensures the complete removal of solvents after the selected membrane drying procedure.~~~~Further~~ Noteworthy, the absence of weight loss at lower temperatures, for both MMMs and pure membranes, ensures the complete removal of solvents after the selected membrane drying procedure.

DSC and CO_2 adsorption measurements were performed on the MMMs to gain further insight into the filler-polymer interface. DSC results show that the T_g of all the MMMs (Table S2) are similar to that of bare Matrimid® (~ 594 K), suggesting that there is no significant rigidification of the polymeric chains around the BILP particles~~,~~. This is in line with ~~like~~ previous~~ly~~ reported results on POF-MMMs [20,46]. To check whether the BILP pores are still available in the MMMs, CO_2 adsorption isotherms were acquired at 273 K for both bare Matrimid® and the prepared MMMs. The incorporation of BILP-101 and RT-BILP-101 into the polymeric matrix results in an enhanced CO_2 uptake, achieving higher CO_2 uptakes compared to pure Matrimid® in all cases (Fig. S7). As expected, the higher the filler loading, the higher the maximum amount of CO_2 that can be adsorbed, indicating that the filler pores are still accessible to CO_2 once the BILP particles have been embedded in the polymeric matrix. ~~In addition, the RT-BILP-101 MMMs can reach almost the same CO_2 uptake compared to BILP-101 MMMs at the same loading.~~ In order to gain further the influence of the filler on the adsorption capacity of the resulting MMMs, the estimated CO_2 uptake for the 16 wt% MMMs calculated as a linear combination of those uptakes for the pure components is shown in Fig. 5, together with the experimentally measured isotherms for that filler loading. Experimentally obtained CO_2 uptakes are somewhat lower than those calculated for both BILP-101 and RT-BILP-101 MMMs, pointing to a partial pore blockage of BILP-101 and RT-BILP-101 by the polymer chains [23,46]. The difference between the estimated CO_2 uptake and the experimental one is larger for BILP-101 MMMs (33.1% porosity loss for BILP-101) than for RT-BILP-101 MMMs (25.8% loss), suggesting that the bigger porosity of BILP-101 is more easily blocked by the polymer.

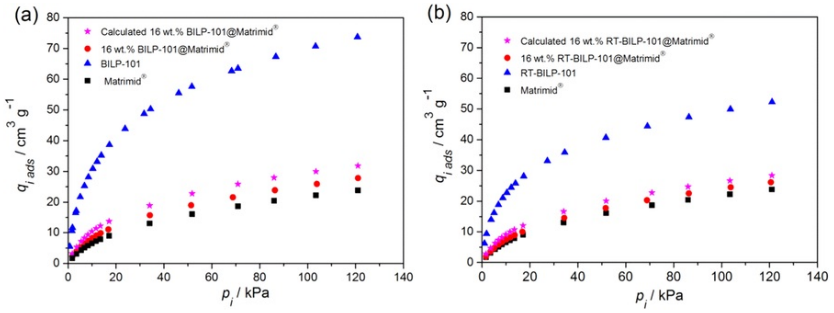

(New figure has been provided for Fig. 5 in which the Y axis is changed) **Fig. 5** CO_2 adsorption isotherms acquired for BILP-101, RT-BILP-101 and the prepared membranes at ~~273~~273 K. The calculated value was obtained by a linear combination of those uptakes for the pure components.

alt-text: Fig. 5

~~This is further supported by the pore size distribution curves of the MMMs calculated from the adsorption branch of CO~~This is further supported by the pore size distribution curves of the MMMs calculated from the adsorption branch of the $CO_{~~2~~2}$ ~~isotherms (~~isotherms (Fig. S8 should read Fig. S8a) (Fig. S8 ~~). Both, BILP-101 and RT-BILP-101-based MMMs showed a drastic reduction in the pore volume once the filler is embedded in Matrimid®, given the dense nature of the latter.~~). Both, BILP-101 and RT-BILP-101-based MMMs showed a drastic reduction in the pore volume once the filler is embedded in Matrimid®, given the dense nature of the latter. (Fig S9 should read Fig S8b) Fig S9 ~~shows however a more pronounced reduction of the pore volume for BILP-101 than for RT-BILP-101 once incorporated in the polymeric matrix. We hypothesize that, together with a reduction in the size of the bigger pores and in the expected CO~~shows however a more pronounced reduction of the pore volume for BILP-101 than for RT-BILP-101 once incorporated in the polymeric matrix. We hypothesize that, together with a reduction in the size of the bigger pores and in the expected $CO_{~~2~~2}$ ~~uptake (~~uptake (~~vide supra~~*vide supra* ~~), this points to the partial blockage of the filler pores, which may take place together with a partial collapse of the BILP-101 porous polymer. As already observed for the CO~~), this points to the partial blockage of the filler pores, which may take place together with a partial collapse of the BILP-101 porous polymer. As already observed for the $CO_{~~2~~2}$ ~~isotherms, this effect is more prominent for BILP-101.~~isotherms, this effect is more prominent for BILP-101.

3.3 Gas separation performance

~~The flat sheet b~~Bare Matrimid® ~~membranes~~ and MMMs containing different loadings (0, 8, 16 and 24 wt%) of BILP-101 and RT-BILP-101 particles were shaped in the form of flat sheets membranes and tested in the separation of CO_2 from a 15:85 CO_2/N_2 gas mixture at 308 K. Besides the effect of the filler porosity on the membrane performance, the influence of the feed pressure was also investigated, and thus varied between 2 and 5 bar. At least 2–3 membranes were tested for each BILP loading in order to provide reliable error estimations. ~~All the prepared membranes can withstand the permeation test conditions, indicating a good mechanical stability of the membranes under relevant conditions for post-combustion capture. Further, in line with the measured~~All the prepared membranes can withstand the permeation test conditions, indicating a good mechanical stability of the membranes under relevant conditions for post-combustion capture. Further, in line with the measured ~~T~~$T_{~~g~~g}$ ~~values, the membranes remain flexible upon 24% BILP-101 and RT-BILP-101 loading (~~values, the membranes remain flexible up to~~n~~ 24% BILP-101 and RT-BILP-101 loading (Fig. S9 ~~)~~).~~-~~Upon addition of BILP particles, the membranes showed an increase in the CO_2 permeability preserving the original CO_2/N_2 mixed gas selectivities (Fig. 6). The gas permeability increases with increasing BILP loading, for both BILP-101 and RT-BILP-101, ~~In this situation t~~ attributed to the ~~he enhanced CO_2 permeability can be attributed to the incorporation of porous fillers into the polymeric matrix, providing~~ additional transport pathways ~~for the permeating gases~~introduced by the incroporation of the filler [46]. Particuarly, for the 24 wt% RT-BILP-101 MMMs, the CO_2 peremeability increased by a factor of 2.8 (from 9.6 to 27.0 Barrer) as compared to bare Matrimid® with constant CO_2/N_2 selectivity. ~~Further, the CO~~Further, ~~t~~The $CO_{~~2~~2}$ ~~adsorption isotherms of all the prepared membranes were fit on the dual-mode model (~~adsorption isotherms of all the prepared membranes were fit on the dual-mode model (Fig. S10 ~~and~~and Table S1~~). These results indicate that the incorporation of both BILP fillers lead to the increase of~~). The~~se~~ results indicate that the incorporation of both BILP fillers lead to the increase of κ_D ~~,~~, C'_H ~~and b simultaneously. The increase in~~and b simultaneously. The increase in C'_H ~~is more significant (~30% increase were achieved for 24wt.% loading MMMs compared to pure Matrimid®), indicating a higher amount of free volume introduced by the BILP fillers.~~is more significant (~ 30% increase were achieved for 24 wt% loading MMMs compared to pure Matrimid®), indicating a higher amount of free volume introduced by the BILP fillers.

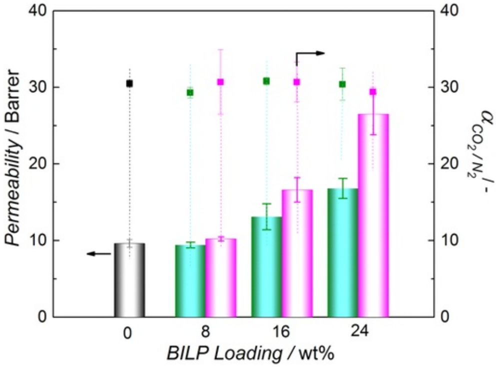

Fig. 6 Performance of MMMs with different BILP-101 and RT-BILP-101 loadings in the separation of CO_2 from a 15:85 CO_2/N_2 mixture at ~~308~~308 K and a feed pressure of ~~2~~2 bar. Grey, green and purple colour correspond to the pure ~~Matrimid®,~~Matrimid®, BILP-101 and RT-BILP-101 MMMs, respectively. Error bars correspond to the standard deviation of different membranes. (For interpretation of the references to color in this figure legend, the reader is referred to the web version of this article.)

alt-text: Fig. 6

It is noteworthy that MMMs fabricated with BILP-101, which possesses a higher BET surface area, showed a lower CO_2 permeability than the RT-BILP-101 MMMs at the same loading. This may originate from the pore blocking by the polymer chains as indicated by CO_2 adsorption (Fig. 5), being more significant for BILP-101 than RT-BILP-101 due to the big porosity and more open pore volume.

~~The gas permeability increases with increasing BILP loading, for both BILP-101 and RT-BILP-101, attributed to the additional transport pathways introduced by the incorporation of the filler. Particularly, for the 24~~24 wt% ~~RT-BILP-101 MMMs, the CO~~$_2$ ~~permeability increased by a factor of 2.8 (from 9.6 to 27 Barrer) as compared to bare Matrimid®~~Matrimid® ~~with constant CO~~$_2$~~/N~~$_2$ ~~selectivity.~~ Fig. 7 shows the influence of feed pressure on the gas permeation performance of the membrane. Both the CO_2 and N_2 permeability of the BILP MMMs are higher than the pure ~~Matrimid®~~Matrimid® through the whole pressure range except for ~~8~~8 wt% loading, which is close to ~~Matrimid®.~~Matrimid®. The CO_2 permeability decreases with increasing feed pressure. This is a well-known for components adsorbing in the nonlinear pressure range. Saturation of Langmuir adsorption sites in zeolites [47,48] and glassy polymers [23,46,49] at higher pressures results in a decrease in the membrane permeability. For the case of ~~24~~24 wt% loading BILP-101 MMMs (see Table S3 for the detailed value, only one low pressure data was put in Fig. 7a for clarity), the presences of small defects play a role at high pressures, leading to the fast diffusion of N_2 and thereby decrease the CO_2/N_2 selectivity significantly.

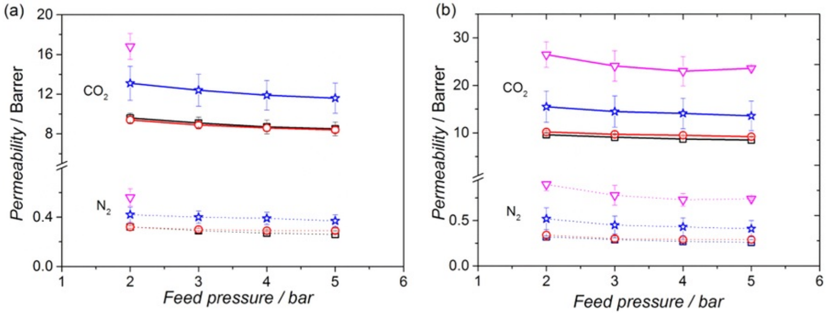

Fig. 7 Effect of the feed pressure on the gas permeation performance of the prepared (a) BILP-101 and (b) RT-BILP-101 membranes. Results obtained in the separation of CO_2 from a 15:85 CO_2/N_2 mixture at ~~308~~308 K. □ Pure ~~Matrimid®,~~Matrimid®, ▯ ~~8~~8 wt% MMMs, ☆ ~~16~~16 wt% MMMs and ∇ ~~24~~24 wt% MMMs.

alt-text: Fig. 7

~~To gain further insight into the long-term membrane performance, 16wt.% loading MMMs (BILP-101 and RT-BILP-101) were re-tested after 4 months (~~To gain further insight into the long-term membrane performance, 16 wt% loading MMMs (BILP-101 and RT-BILP-101) were re-tested after 4 months (Table S4~~), indicating that the separation performance was maintained. As expected, a slight decrease in the membrane permeability was observed, from 17.0 to 15.1 Barrer and from 13.0 to 11.3 Barrer for RT-BILP-101 and BILP-101-based MMMs, respectively, while keeping a relatively constant selectivity. This decrease in permeability is related to a decrease in the excess free volume of glassy polymers after physical aging.~~), indicating that the separation performance was maintained. As expected, a slight decrease in the membrane permeability was observed, from 17.0 to 15.1 Barrer and from 13.0 to 11.3 Barrer for RT-BILP-101 and BILP-101-based MMMs, respectively, while keeping a relatively constant selectivity. This decrease in permeability is related to a decrease in the excess free volume of glassy polymers after physical aging.

~~Considering the practical post-combustion CO~~Considering the practical post-combustion CO~~2~~$_2$ ~~capture process, the flue gas needs to be reheated to prevent corrosion problems caused by water vapour condensation in the stack~~capture process, the flue gas needs to be reheated to prevent corrosion problems caused by water vapor condensation in the stack [50]~~. Thus, the effect of temperature (308–358K) on gas separation performance was further investigated to better understand the actual performance of BILP MMMs in real industrial applications. The gas permeability increases with increasing temperature while this is accompanied by a decrease in the CO~~. Thus, the effect of temperature (308–358 K) on gas separation performance was further investigated to better understand the actual performance of BILP MMMs in real industrial applications. The gas permeability increases with increasing temperature while this is accompanied by a decrease in the CO~~2~~$_2$~~/N~~/N~~2~~$_2$ ~~selectivity for both BILP MMMs (~~selectivity for both BILP MMMs (Table S5~~). To better understand this, Arrhenius equation was applied to calculate the activation energy (~~). To shed some light on this behaviour~~better understand this~~, Arrhenius equation was applied to calculate the activation energy (~~E~~E_p~~) for permeation (~~) for permeation (Fig. 8~~).~~)~~.~~

$$P_i = P_{i,0} \exp\left(\frac{-E_{P,i}}{RT}\right) \quad (4)$$

where $E_{P,i}$, P_i and $P_{i,0}$ represent the activation energy, the gas permeability and the pre-exponential factor of a gas component *i*, respectively, *T* is the absolute temperature and *R* is the ideal gas constant. Similarly to zeolite membranes [51], the activation energy, E_P, is determined by two ~~principle~~main factors: the penetrants molecular size, which affects diffusivity, and the interaction with the polymer matrix, related to the penetrants' solubility, and is given by the following equation:

$$E_p = E_d + \Delta H_s \quad (5)$$

where E_d is the required energy for diffusion and increases with the penetrants' molecular size, being positive for a diffusion activated processes, and ΔH_s is the heat of adsorption, being more negative for more soluble gases.

An increase of temperature therefore results in two counteractive effects: on the one hand side, the gas solubility decreases, being this effect more pronounced for the more soluble gas, *i.e.* CO_2; on the other hand, the diffusivity increases, being this enhancement larger for the penetrant with the higher molecular size, *i.e.* N_2. This increase in diffusivity is related to a positive E_d, implying a diffusion activated processes, together with a higher mobility of the polymer segmental chains [52,53]. Overall, the diffusivity increase dominates, resulting in an enhanced permeability for both, CO_2 and N_2. This permeability increase is higher for N_2, leading to a decrease in the resultant permselectivity (Table S5). This is in line with the calculated E_p activation energy values (Table 1): the positive values results into an increase of the gas permeability with temperature, this enhancement being larger for the penetrant with a higher E_p, *i.e.* N_2.

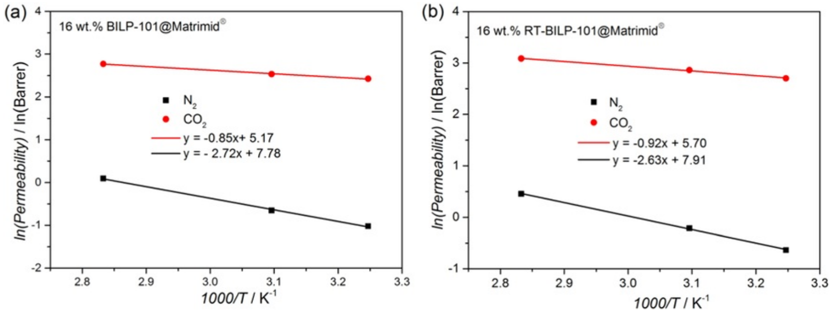

Fig. 8 Effect of operating temperature on CO_2 and N_2 permeability of aged (a) ~~16~~16 wt% BILP-101 and (b) ~~RT-BILP-101@Matrimid®~~RT-BILP-101@Matrimid® at 2 feed bar pressure (solid lines represent the Arrhenius plot).

alt-text: Fig. 8

Table 1 Activation energies for the permeation of CO_2 and N_2 in aged ~~16~~16 wt% BILP MMMs at ~~2~~2 bar feed pressure.

alt-text: Table 1

Membrane	E_p ~~(kJ mol~~(kJ mol~~$^{-1}$~~$^{-1}$)	
	CO_2	**N_2**
Aged ~~16~~16 wt% BILP-101 MMMs @ ~~Matrimid®~~Matrimid®	**7.1**	**22.6**
Aged ~~16~~16 wt%~~wt.% RT-BILP-101 @~~ RT-BILP-101 @ Matrimid®	**7.7**	**21.9**

~~Finally, the separation performance of BILP-101 and RT-BILP-101-based MMMs were compared with the Robeson upper bound together with the performance of other reported POF-containing MMMs (~~Finally, the separation performance of BILP-101 and RT-BILP-101-based MMMs were compared with the Robeson upper bound together with the performance of other reported POF-containing MMMs (Fig. 9 ~~and~~and Table S6~~). The performance of the MMMs prepared in this study is located in the same region as the membranes reported with other POF fillers, such as ACOF-1 or BILP-4. Although a significant increase in CO~~). The performance of the MMMs prepared in this study is located in the same region as the membranes reported with other POF fillers, such as ACOF-1 or BILP-4. Although a significant increase in CO~~$_2$~~$_2$ ~~permeability was achieved by incorporating RT-BILP-101 fillers in Matrimid®, the overall performance still stays below the upper bound limit due to the low permeability of pure Matrimid®. Our results are therefore in line with other POF-based MMMs prepared with low permeable polymers, for which by adding the filler the gas permeability can be typically increased while scarifying or maintaining the selectivity.~~permeability was achieved by incorporating RT-BILP-101 fillers in Matrimid®, the overall performance still ~~stay~~lies below the upper bound limit due to the low permeability of pure Matrimid®. Our results are therefore in line with other POF-based MMMs prepared with low permeable polymers, for which by adding the filler the gas permeability can be typically increased while s~~carifying~~acrificing or maintaining the selectivity.

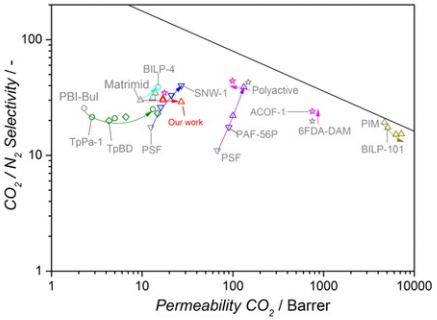

Fig. 9 Robeson plot for CO_2/N_2 separation, showing the gas separation performance of the prepared BILPs-based MMMs (represented by red triangles and corresponding to 16 and ~~24~~24 wt% filler loading). Most relevant results reported in literature for POF-based MMMs are also included for comparison (Table S6). The black line corresponds to the 2008 Robeson bound line and the arrows indicate the trend of separation performance from pure polymer to POF based MMMs. (For interpretation of the references to color in this figure legend, the reader is referred to the web version of this article.)

alt-text: Fig. 9

4 Conclusions

Porous BILPs with different porosities (BILP-101 and RT-BILP-101) were prepared and dispersed in ~~Matrimid®~~Matrimid® to prepare MMMs. Their structure~~s~~ and performance were compared in this study. Through controlling the initial polymerization rate, RT-BILP-101 with lower porosity than BILP-101 was synthesized~~ than BILP-101~~. DRIFTS and ^{13}C CP-CMS NMR measurements confirm~~s~~ the same chemical connectivity ~~of two~~for both BILPs. In the MMMs, a good dispersion and adhesion between the fillers and the polymer matrix was obtained. No rigidification was observed for the polymer chains after incorporating ~~both BILPs~~the different fillers. The incorporation of both BILPs into ~~Matrimid®~~Matrimid® enhanced the gas permeability ~~for both~~ CO_2 and N_2, while keeping the mixed gas selectivity constant. The permeability increases with increasing the filler loading attributed to the fast diffusion pathways introduced by the porous BILP network, while the polymer still controls the selectivity. Besides, MMMs fabricated with RT-BILP-101 exhibits higher gas permeability than BILP-101 MMMs at the same loading, due to the lower partial pore blockage of the porosity by the polymer in the MMMs.

Overall, our results demonstrate that the porosity of the filler has an impact on the MMM's permeation performance and should be helpful for the design of POF-based MMMs considering ~~that~~ the relatively large POF pores for gas separation.

Acknowledgements

B.S. gratefully acknowledges the Netherlands National Science Foundation (NWO) for her personal VENI grant. M.S. gratefully acknowledges the support from the China Scholarship Council.

Appendix A. ~~Supporting information~~Supplementary material

Supplementary data associated with this article can be found in the online version at doi:10.1016/j.memsci.2018.08.023.

References

[1] Y.-S. Bae and R.Q. Snurr, Development and evaluation of porous materials for carbon dioxide separation and capture, ~~*Angewandte Chemie International Edition*~~*Angew. Chem. Int. Ed.* **50**, 2011, 11586–11596.

[2] L.M. Robeson, The upper bound revisited, ~~*Journal of Membrane Science*~~*J. Membr. Sci.* **320**, 2008, 390–400.

[3] H.B. Park, J. Kamcev, L.M. Robeson, M. Elimelech and B.D. Freeman, Maximizing the right stuff: ~~The~~the trade-off between membrane permeability and selectivity, *Science* **356**, 2017, eaab0530.

[4] A. Bos, I. Pünt, H. Strathmann and M. Wessling, Suppression of gas separation membrane plasticization by homogeneous polymer blending, *AIChE* ~~*Journal*~~*J.* **47**, 2001, 1088–1093.

[5] X.Y. Chen, V.-T. Hoang, D. Rodrigue and S. Kaliaguine, Optimization of continuous phase in amino-functionalized metal-organic framework (MIL-53) based co-polyimide mixed matrix membranes for CO_2/CH_4 separation *RSC* ~~*Advances*~~*Adv.* **3**, 2013, 24266–24279.

[6] S.H. Han, J.E. Lee, K.-J. Lee, H.B. Park and Y.M. Lee, Highly gas permeable and microporous polybenzimidazole membrane by thermal rearrangement, ~~*Journal of Membrane Science*~~*J. Membr. Sci.* **357**, 2010, 143–151.

[7] P. Gorgojo, S. Karan, H.C. Wong, M.F. Jimenez-Solomon, J.T. Cabral and A.G. Livingston, Ultrathin polymer films with intrinsic microporosity: ~~Anomalous~~anomalous solvent permeation and high flux membranes, ~~*Advanced Functional Materials*~~*Adv. Funct. Mater.* **24**, 2014, 4729–4737.

[8] M. Carta, R. Malpass-Evans, M. Croad, Y. Rogan, J.C. Jansen, P. Bernardo, F. Bazzarelli and N.B. McKeown, An efficient polymer molecular sieve for membrane gas separations, *Science* **339**, 2013, 303–307.

[9] I. Kiesow, D. Marczewski, L. Reinhardt, M. Mühlmann, M. Possiwan and W.A. Goedel, Bicontinuous zeolite polymer composite membranes prepared via float casting, ~~*Journal of the American Chemical Society*~~*J. Am. Chem. Soc.* **135**, 2013, 4380–4388.

[10] T.W. Pechar, S. Kim, B. Vaughan, E. Marand, M. Tsapatsis, H.K. Jeong and C.J. Cornelius, Fabrication and characterization of polyimide–zeolite L mixed matrix membranes for gas separations, ~~*Journal of Membrane Science*~~*J. Membr. Sci.* **277**, 2006, 195–202.

[11] T. Rodenas, M. van Dalen, E. García-Pérez, P. Serra-Crespo, B. Zornoza, F. Kapteijn and J. Gascon, Visualizing MOF mixed matrix membranes at the nanoscale: towards structure-performance relationships in CO_2/CH_4 separation over NH_2-MIL-53(Al)@PI, ~~*Advanced Functional Materials*~~*Adv. Funct. Mater.* **24**, 2014, 249–256.

[12] T. Rodenas, I. Luz, G. Prieto, B. Seoane, H. Miro, A. Corma, F. Kapteijn, F.X. Llabrés, I. Xamena and J. Gascon, Metal–organic framework nanosheets in polymer composite materials for gas separation, ~~*Nature Materials*~~*Nat. Mater.* **14**, 2015, 48–55.

[13] L. Zou, Y. Sun, S. Che, X. Yang, X. Wang, M. Bosch, Q. Wang, H. Li, M. Smith, S. Yuan, Z. Perry and H.C. Zhou, Porous organic polymers for post-combustion carbon capture, ~~*Advanced Materials*~~*Adv. Mater.* **29**, 2017, 1700229.

[14] X. Feng, X. Ding and D. Jiang, Covalent organic frameworks, ~~*Chemical Society Reviews*~~*Chem. Soc. Rev.* **41**, 2012, 6010–6022.

[15] S.-Y. Ding and W. Wang, Covalent organic frameworks (COFs): from design to applications, ~~*Chemical Society Reviews*~~*Chem. Soc. Rev.* **42**, 2013, 548–568.

[16] Y. Xu, S. Jin, H. Xu, A. Nagai and D. Jiang, Conjugated microporous polymers: design, synthesis and application, ~~*Chemical Society Reviews*~~*Chem. Soc. Rev.* **42**, 2013, 8012–8031.

[17] H. Ma, H. Ren, X. Zou, S. Meng, F. Sun and G. Zhu, Post-metalation of porous aromatic frameworks for highly efficient carbon capture from CO_2+N_2 and CH_4+N_2 ~~mixtures, Polymer Chemistry~~mixtures, *Polym. Chem.,* **5**, 2014, 144–152.

[18] A. Bhunia, I. Boldog, A. Moller and C. Janiak, Highly stable nanoporous covalent triazine-based frameworks with an adamantane core for carbon dioxide sorption and separation, ~~*Journal of Materials Chemistry*~~ *J. Mater. Chem. A* **1**, 2013, 14990–14999.

[19] X. Wu, Z. Tian, S. Wang, D. Peng, L. Yang, Y. Wu, Q. Xin, H. Wu and Z. Jiang, Mixed matrix membranes comprising polymers of intrinsic microporosity and covalent organic framework for gas separation, ~~*Journal of Membrane Science*~~*J. Membr. Sci.* **528**, 2017, 273–283.

[20] T.D.M. Tessema, S.R. Venna, G. Dahe, D.P. Hopkinson, H.M. El-Kaderi and A.K. Sekizkardes, Incorporation of benzimidazole linked polymers into Matrimid to yield mixed matrix membranes with enhanced CO_2/N_2 selectivity, ~~*Journal of Membrane Science*~~*J. Membr. Sci.* **554**, 2018, 90–96.

[21] C. Zou, Q. Li, Y. Hua, B. Zhou, J. Duan and W. Jin, Mechanical synthesis of COF nanosheet cluster and its mixed matrix membrane for efficient CO_2 removal, *ACS* ~~*Applied Materials &*~~ *Appl. Mater. Interfaces* **9**, 2017, 29093–29100.

[22] L. Meng, X. Zou, S. Guo, H. Ma, Y. Zhao and G. Zhu, ~~Self Supported~~Self-supported fibrous porous aromatic membranes for efficient CO_2/N_2 separations, *ACS* ~~*Applied Materials &*~~ *Appl. Mater. Interfaces* 2015.

[23] M. Shan, B. Seoane, E. Rozhko, A. Dikhtiarenko, G. Clet, F. Kapteijn and J. Gascon, Azine-linked covalent organic framework (COF)-based mixed-matrix membranes for CO_2/CH_4 separation, ~~*Chemistry-A European Journa*~~*Chem.-Eur. J.* **22**, 2016, 14467–14470.

[24] M.G. Rabbani and H.M. El-Kaderi, Template-free synthesis of a highly porous benzimidazole-linked polymer for CO_2 capture and H_2 storage, ~~*Chemistry of Materials*~~*Chem. Mater.* **23**, 2011, 1650–1653.

[25] C. Klumpen, F. Radakovitsch, A. Jess and J. Senker, BILP−19—An ultramicroporous organic network with exceptional carbon dioxide uptake, *Molecules* **22**, 2017, 1343.

[26] M.G. Rabbani and H.M. El-Kaderi, Synthesis and characterization of porous benzimidazole-linked polymers and their performance in small gas storage and selective uptake, ~~*Chemistry of Materials*~~*Chem. Mater.* **24**, 2012, 1511–1517.

[27] A.K. Sekizkardes, V.A. Kusuma, G. Dahe, E.A. Roth, L.J. Hill, A. Marti, M. Macala, S.R. Venna and D. Hopkinson, Separation of carbon dioxide from flue gas by mixed matrix membranes using dual phase microporous polymeric constituents, ~~*Chemical Communications*~~*Chem. Commun.* **52**, 2016, 11768–11771.

[28] L. Zou, Y. Sun, S. Che, X. Yang, X. Wang, M. Bosch, Q. Wang, H. Li, M. Smith, S. Yuan, Z. Perry and H.-C. Zhou, Porous organic polymers for post-combustion carbon capture, ~~*Advanced Materials*~~*Adv. Mater.* **29**, 2017, 1700229

[29] X. Zou, G. Zhu, Microporous organic materials for membrane-based gas separation, ~~Advanced Materials,~~ Adv. Mater., p. 1700750.

[30] L. Ge, W. Zhou, V. Rudolph and Z. Zhu, Mixed matrix membranes incorporated with size-reduced Cu-BTC for improved gas separation, ~~*Journal of Materials Chemistry*~~ *J. Mater. Chem. A* **1**, 2013, 6350–6358.

[31] J. Dechnik, J. Gascon, C. Doonan, C. Janiak and C.J. Sumby, Mixed-matrix membranes, ~~*Angewandte Chemie International Edition*~~*Angew. Chem. Int. Ed.* **129**, 2017, 9420–9439.

[32] J. Sánchez-Laínez, B. Zornoza, S. Friebe, J. Caro, S. Cao, A. Sabetghadam, B. Seoane, J. Gascon, F. Kapteijn, C. Le Guillouzer, G. Clet, M. Daturi, C. Téllez and J. Coronas, Influence of ZIF-8 particle size in the performance of polybenzimidazole mixed matrix membranes for pre-combustion CO$_2$ capture and its validation through interlaboratory test, ~~*Journal of Membrane Science*~~*J. Membr. Sci.* **515**, 2016, 45–53.

[33] A. Sabetghadam, B. Seoane, D. Keskin, N. Duim, T. Rodenas, S. Shahid, S. Sorribas, C.L. Guillouzer, G. Clet and C. Tellez, Metal ~~Organic Framework Crystals~~organic framework crystals in ~~Mixed-Matrix Membranes: Impact~~mixed-matrix membranes: impact of the ~~Filler Morphology~~filler morphology on the ~~Gas Separation Performance~~gas separation performance, ~~*Advanced Functional Materials*~~*Adv. Funct. Mater.* **26**, 2016, 3154–3163.

[34] M.W. Anjum, F. Vermoortele, A.L. Khan, B. Bueken, D.E. De Vos and I.F.J. Vankelecom, Modulated UiO-66 based ~~Mixed Matrix Membranes~~mixed matrix membranes for CO$_2$ ~~Separation~~separation, *ACS* ~~*Applied Materials &*~~ *Appl. Mater. Interfaces* **45**, 2015, 25193–25201.

[35] A.K. Sekizkardes, J.T. Culp, T. Islamoglu, A. Marti, D. Hopkinson, C. Myers, H.M. El-Kaderi and H.B. Nulwala, An ultra-microporous organic polymer for high performance carbon dioxide capture and separation, ~~*Chemical Communications*~~*Chem. Commun.* **51**, 2015, 13393–13396.

[36] B. Zornoza, A. Martinez-Joaristi, P. Serra-Crespo, C. Tellez, J. Coronas, J. Gascon and F. Kapteijn, Functionalized flexible MOFs as fillers in mixed matrix membranes for highly selective separation of CO$_2$ from CH$_4$ at elevated pressures, ~~*Chemical Communications*~~*Chem. Commun.* **47**, 2011, 9522–9524.

[37] S. Altarawneh, T. İslamoğlu, A.K. Sekizkardes and H.M. El-Kaderi, Effect of acid-catalyzed formation rates of benzimidazole-linked polymers on porosity and selective CO$_2$ capture from gas mixtures, ~~*Environmental Science & Technology*~~*Environ. Sci. Technol.* **49**, 2015, 4715–4723.

[38] P. Totsatitpaisan, S.P. Nunes, K. Tashiro and S. Chirachanchai, Investigation of the role of benzimidazole-based model compounds on thermal stability and anhydrous proton conductivity of sulfonated poly(ether ~~ether ketone)~~ether ketone), *Solid State* ~~*Ionics*~~*Ion.* **180**, 2009, 738–745.

[39] P. Pandey, A.P. Katsoulidis, I. Eryazici, Y. Wu, M.G. Kanatzidis and S.T. Nguyen, Imine-linked microporous polymer organic frameworks, ~~*Chemistry of Materials*~~*Chem. Mater.* **22**, 2010, 4974–4979.

[40] F. Svec and J.M. Frechet, Kinetic control of pore formation in macroporous polymers. Formation of" molded" porous materials with high flow characteristics for separations or catalysis, ~~*Chemistry of Materials*~~*Chem. Mater.* **7**, 1995, 707–715.

[41] H. Furukawa and O.M. Yaghi, Storage of hydrogen, methane, and carbon dioxide in highly porous covalent organic frameworks for clean energy applications, ~~*Journal of the American Chemical Society*~~*J. Am. Chem. Soc.* **131**, 2009, 8875–8883.

[42] M. Zhang, Z. Perry, J. Park and H.-C. Zhou, Stable benzimidazole-incorporated porous polymer network for carbon capture with high efficiency and low cost, *Polymer* **55**, 2014, 335–339.

[43] T. Ben, C. Pei, D. Zhang, J. Xu, F. Deng, X. Jing and S. Qiu, Gas storage in porous aromatic frameworks (PAFs), *Energy* ~~*& Environmental Science*~~*Environ. Sci.* **4**, 2011, 3991–3999.

[44] R. Dawson, D.J. Adams and A.I. Cooper, Chemical tuning of CO_2 sorption in robust nanoporous organic polymers, *~~Chemical Science~~Chem. Sci.* **2**, 2011, 1173–1177.

[45] A.K. Sekizkardes, T. Islamoglu, Z. Kahveci and H.M. El-Kaderi, Application of pyrene-derived benzimidazole-linked polymers to CO_2 separation under pressure and vacuum swing adsorption settings, *~~Journal of Materials Chemistry~~ J. Mater. Chem. A* **2**, 2014, 12492–12500.

[46] M. Shan, B. Seoane, E. Andres-Garcia, F. Kapteijn and J. Gascon, Mixed-matrix membranes containing an azine-linked covalent organic framework: ~~Influence~~influence of the polymeric matrix on post-combustion CO_2-capture, *~~Journal of Membrane Science~~J. Membr. Sci.* **549**, 2018, 377–384.

[47] J.M. van de Graaf, F. Kapteijn and J.A. Moulijn, Methodological and operational aspects of permeation measurements on silicalite−1 membranes, *~~Journal of Membrane Science~~J. Membr. Sci.* **144**, 1998, 87–104.

[48] A. Cybulski and J.A. Moulijn, Structured ~~catalysts~~Catalysts and ~~reactors~~Reactors, 2005, CRC press; Boca Raton, FL, USA.

[49] T. Li, Y. Pan, K.-V. Peinemann and Z. Lai, Carbon dioxide selective mixed matrix composite membrane containing ZIF-7 nano-fillers, *~~Journal of Membrane Science~~J. Membr. Sci.* **425–426**, 2013, 235–242.

[50] H.Z. Chen, Z. Thong, P. Li and T.-S. Chung, High performance composite hollow fiber membranes for CO_2/H_2 and CO_2/N_2 separation, *~~International Journal of Hydrogen~~ Int. J. Hydrog. Energy* **39**, 2014, 5043–5053.

[51] K. Freek, ~~vdG.J.~~v.d.G.J. ~~M.~~M and M.J. ~~A.~~A, One-component permeation maximum: ~~Diagnostic~~diagnostic tool for silicalite−1 membranes?, *AIChE ~~Journal~~J.* **46**, 2000, 1096–1100.

[52] A.L. Khan, X. Li and I.F.J. Vankelecom, ~~SPEEK/Matrimid~~SPEEK/matrimid blend membranes for CO_2 separation, *~~Journal of Membrane Science~~J. Membr. Sci.* **380**, 2011, 55–62.

[53] A. Ebadi Amooghin, M. Omidkhah and A. Kargari, Enhanced CO_2 transport properties of membranes by embedding nano-porous zeolite particles into Matrimid®5218 matrix, *RSC ~~Advances~~Adv.* **5**, 2015, 8552–8565.

Appendix A. Supplementary material

Multimedia Component 1

Supplementary material. (Replace Figure S7 (see attached))

Graphical abstract

Filler porosity plays a key role in designing benzimidazole linked polymers (BILPs)-MMMs for CO_2/N_2 ~~separation~~separation.

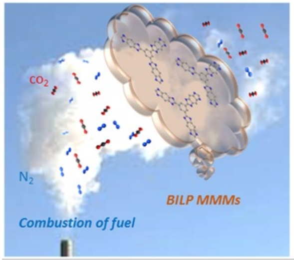

alt-text: fx1

Highlights

- Benzimidazole-linked polymers (BILPs) with two different porosities were successfully synthesized through controlling the initial polymerization rate.
- Both BILPs showed good adhesion with the ~~Matrimid®~~Matrimid® polymeric matrix as confirmed by SEM.

- The incorporation of both BILP fillers into ~~Matrimid®~~Matrimid® enhanced the gas permeability at constant selectivity.
- This study investigates for the first time the influence of the filler porosity on the performance of POF-containing mixed matrix membranes.

Queries and Answers

Query:

Please confirm that given names and surnames have been identified correctly and are presented in the desired order, and please carefully verify the spelling of all authors.

Answer: Done

Query:

Your article is registered as a regular item and is being processed for inclusion in a regular issue of the journal. If this is NOT correct and your article belongs to a Special Issue/Collection please contact k.narasimhan@elsevier.com immediately prior to returning your corrections.

Answer: It is correct, this article is a regular item

Query:

Corresponding author has not been indicated in the author group. Kindly provide the corresponding author's information.

Answer: Corresponding authors: Beatriz Seoane (b.seoanedelacuesta@uu.nl, Inorganic Chemistry and Catalysis group, Debye Institute for Nanomaterials Science, Utrecht University, Universiteitsweg 99, Utrecht 3584 CG, The Netherlands) and Jorge Gascon (jorge.gascon@kaust.edu.sa, King Abdullah University of Science and Technology, KAUST Catalysis Center, Advanced Catalytic Materials, Thuwal 23955, Saudi Arabia)

Query:

Highlights should only consist of 85 characters per bullet point, including spaces. The highlights provided are too long; please edit them to meet the requirement.

Answer: 1. Benzimidazole-linked polymers (BILPs) with two different porosities were synthesized.
2. Both BILPs showed good adhesion with the Matrimid® polymeric matrix.
3. The incorporation of both BILP fillers into Matrimid® enhanced the gas permeability.
4. The filler porosity plays a role in the performance of POF-containing MMMs.
Attachments: Highlights.doc

Query:

"Figs. 6 and 9" have been submitted as color images; however, the captions have been reworded to ensure that they are meaningful when your article is reproduced both in color and in black and white. Please validate if the changes made are ok.

Answer: ok

Query:

Please type the full funder name and country, plus grant IDs in the text, if available. Correctly acknowledging the primary funders and grant IDs of your research is important to ensure compliance with funder policies. Have we correctly interpreted the following funding source(s) you cited in your article: "Netherlands National Science Foundation, The Netherlands" and "China Scholarship Council, China"?

Answer: The acknowledgements should read: B.S. gratefully acknowledges the Dutch National Science Foundation (NWO), The Netherlands, for her personal VENI grant 722.015.007. M. S. gratefully acknowledges the support from the Cina Scholarship Council.